Monthly Notices of the ROYAL ASTRONOMICAL SOCIETY

MNRAS **539,** 2409–2423 (2025) https://doi.org/10.1093/mnras/staf641
Advance Access publication 2025 April 18

No evidence (yet) for increased star-formation efficiency at early times

C. T. Donnan ,★ J. S. Dunlop, R. J. McLure, D. J. McLeod and F. Cullen
Institute for Astronomy, University of Edinburgh, Royal Observatory, Edinburgh EH9 3HJ, UK

Accepted 2025 April 15. Received 2025 April 7; in original form 2025 January 6

ABSTRACT

Early *JWST* observations have revealed substantial numbers of galaxies out to redshifts as high as $z \simeq 14$, reflecting a slow evolution of the galaxy ultraviolet (UV) luminosity function (LF) not anticipated by many models of galaxy evolution. The discovery of fairly massive galaxies at early times has again been viewed as a challenge to our understanding of early galaxy growth or even Lambda cold dark matter (ΛCDM) cosmology. Here, we develop and test a simple theoretical model which shows that these observations are unsurprising, but instead are arguably as expected if one assumes a non-evolving halo-mass dependent galaxy-formation efficiency consistent with that observed today. Crucially, this model matches the observed galaxy UV LF at $z \simeq 6-13$ *and* the galaxy stellar mass function (GSMF) at $z \simeq 6-8$. Using new constraints on Lyman continuum escape and the ionizing photon production efficiency, we also predict the progress of cosmic hydrogen reionization consistent with current observations. The requirement to fit both the UV LF and the GSMF breaks the degeneracy between mass-to-light ratio and star-formation efficiency, where the typical mass-to-light ratio of galaxies increases systematically with redshift beyond $z \simeq 6$. However, at present this does not require changes to the initial mass function (IMF), cosmic dust, or any other new astrophysics. Rather, the current data can be reproduced simply by assuming ever-younger stellar populations consistent with a formation epoch at $z \simeq 15$. A key prediction of our model therefore is that there should be a more rapid drop-off in the galaxy number density beyond $z \simeq 15$, where one can no longer appeal to ever younger ages to offset the precipitous descent of the halo mass function.

Key words: galaxies: evolution – galaxies: formation – galaxies: high-redshift.

1 INTRODUCTION

In only its first 2 yr of operation, *JWST* has already significantly advanced our knowledge of galaxy evolution back into the first 500 Myr of cosmic time, producing a wealth of new observational results which have revolutionized, and in some cases challenged our understanding of early galaxy formation and growth.

Thanks to its sensitivity and extended near-infrared wavelength coverage (out to $\lambda \simeq 5\,\mu$m) the Near Infrared Camera (NIRCam) instrument on *JWST* has produced the first robust detections of significant numbers of galaxies at redshifts $z > 10$ (e.g. Adams et al. 2022; Castellano et al. 2022; Naidu et al. 2022; Harikane et al. 2023; Donnan et al. 2023a, b; Finkelstein et al. 2023). This has in turn enabled the first robust measurements of the evolving galaxy ultraviolet (UV) luminosity function (LF) at $z = 9-15$, revealing a perhaps surprisingly gradual evolution of the LF over this redshift range (e.g. Adams et al. 2023; Pérez-González et al. 2023; Donnan et al. 2024; McLeod et al. 2024). A number of the new high-redshift galaxy candidates have also been spectroscopically confirmed using the Near Infrared Spectrograph (NIRSpec) instrument (now up to $z \simeq 14.2$) (e.g. Arrabal Haro et al. 2023; Bunker et al. 2023; Curtis-Lake et al. 2023; Carniani et al. 2024a) as well as the Atacama Large Millimeter/submillimeter Array (ALMA) (Schouws et al. 2024).Although the relatively slow evolution of the galaxy population out to extreme redshifts is consistent with some pre-*JWST* predictions from simulations (Wilkins et al. 2023) and observational extrapolations (McLeod, McLure & Dunlop 2016), it is undeniably in tension with a number of pre-*JWST* models, particularly at the bright end (e.g. Mason, Trenti & Treu 2015; Tacchella et al. 2018; Yung et al. 2019).

Several alterations to the physical properties of galaxies at early times have been proposed in order to explain the high-redshift evolution of the galaxy UV LF. First, changes in the star-formation efficiency as a function of redshift have been invoked. For example Harikane et al. (2023) suggest that a constant efficiency model (based on that from Harikane et al. 2022) is unable to match the cosmic star-formation rate density ($\rho_{\rm SFR}$) at $z > 10$. The implication is that an increase in star-formation efficiency with increasing redshift is required in order to match the observed prevalence of UV-luminous galaxies at $z \geq 10$.

Secondly, much reduced dust attenuation has been suggested to explain the bright-end of the UV LF at $z = 11$ (e.g. Ferrara, Pallottini & Dayal 2023) with it being proposed that any dust created in early galaxies could possibly (at least temporarily) be ejected due to the extreme physical conditions associated with early galaxy formation. A lack of dust at extreme redshifts is also consistent with measurements of the UV continuum slopes of galaxies at $z = 11$ (derived from *JWST*/NIRCam photometry) which are, on average,

★ E-mail: callum.donnan@ed.ac.uk

© 2025 The Author(s).
Published by Oxford University Press on behalf of Royal Astronomical Society. This is an Open Access article distributed under the terms of the Creative Commons Attribution License (https://creativecommons.org/licenses/by/4.0/), which permits unrestricted reuse, distribution, and reproduction in any medium, provided the original work is properly cited.

Downloaded from https://academic.oup.com/mnras/article/539/3/2409/8116291 by DESY-Zentralbibliothek user on 07 May 2025

consistent with $\beta \simeq -2.5$ (e.g. Morales et al. 2023; Topping et al. 2023; Cullen et al. 2024).

Another fundamental scaling relation is the galaxy stellar mass function (GSMF) which directly traces the product of star formation across cosmic time. By measuring the GSMF, one can obtain a direct probe of past star formation which, given the relatively short time-scales involved at high redshifts, can be related to star-formation efficiency as a function of dark matter halo mass. Precise measurement of the GSMF requires photometry of the rest-frame optical light from galaxies in order to provide accurate stellar mass measurements for individual galaxies. Using *Hubble Space Telescope* (*HST*) as well as ground-based observations, the GSMF was previously measured up to $z \simeq 3$ by a number of studies (e.g. Muzzin et al. 2013; Mortlock et al. 2015; McLeod et al. 2021; Weaver et al. 2023). However, at $z \geq 3$, measurements of the GSMF proved more challenging because, prior to the launch of *JWST*, this could only be achieved using relatively low resolution *Spitzer* Infrared Array Camera (IRAC) observations to probe the rest-frame optical at higher redshifts (e.g. Grazian et al. 2015; Song et al. 2016; Stefanon et al. 2021). However, now *JWST* has enabled a number of new measurements of the GSMF, with the sensitivity and exquisite angular resolution of NIRCam at $\lambda \simeq 1-5\,\mu$m enabling the first robust measurements of the GSMF over the redshift range $z = 3-8$ (Harvey et al. 2024; Shuntov et al. 2025; Weibel et al. 2024). The discovery of at least some very massive galaxies at these early times has again led to the suggestion that increases in star-formation efficiency are required to explain their existence (e.g. $\epsilon \sim 0.2$; Chworowsky et al. 2024), with some authors even suggesting that the most extreme examples present a challenge to the standard Lambda cold dark matter (ΛCDM) cosmological model (e.g. $\epsilon \sim 0.8-1.0$; Labbé et al. 2023; Glazebrook et al. 2024; Shuntov et al. 2025).

Finally, there have been suggestions that there is an ionizing photon budget crisis (Muñoz et al. 2024) in the sense that some recent *JWST* results appear to imply that too many ionizing photons were produced at early times to be consistent with measurements of the evolving neutral fraction of the intergalactic medium (e.g. Nakane et al. 2024; Tang et al. 2024) including the requirement that reionization is not fully completed until $z \simeq 5.5$ (Bosman et al. 2021).

Given the recent advances in the observational determinations of both the UV LF and the GSMF, it is clearly important to generate a theoretical framework that can simultaneously explain the form and evolution of both of these fundamental scaling relations. In this paper, we expand upon and further develop the model introduced in Donnan et al. (2024) to explore whether a simple theoretical model can reproduce the *JWST* constraints on the UV LF, the GSMF, and the timeline of reionization at $z = 6-13$. This can be viewed as a test of the extent to which current observational data really do require the introduction of more complex/changing astrophysics to explain the new results on early galaxy evolution emerging from *JWST*.

The paper is structured as follows. In Section 2, we initially model the GSMF and compare to the latest observational constraints. In Section 3, we further develop the model to generate the UV LF at $z = 6-13$. In Section 4, we then introduce dust attenuation to our model of the UV LF and present the implied UV attenuation−stellar mass relation. In Section 5, we then explore the predictions of our model for the progress of cosmic hydrogen reionization. In Section 6, we then discuss the implications of our theoretical model for star-formation efficiency, high-mass feedback, dust attenuation, and the ionizing photon budget. Finally, in Section 7 we summarize our conclusions. Throughout we use magnitudes in the AB system (Oke 1974; Oke & Gunn 1983), a Chabrier (2003) initial mass function, and assume a standard cosmological model with $H_0 = 70$ km s^{-1} Mpc^{-1}, $\Omega_m = 0.3$ and $\Omega_\Lambda = 0.7$.

2 MODELLING THE STELLAR MASS FUNCTION

2.1 The star-formation efficiency

We begin by constructing a model of the GSMF which we describe in this section. To construct this simple model we first calculate the evolving dark matter halo mass function (HMF) using HMFCALC (Murray, Power & Robotham 2013) where we use the model of Reed et al. (2007). A number of alternative models of the HMF are available which scatter across a range of ∼0.15 dex at $z = 0$. This scatter increases with redshift with a ∼0.35 dex scatter at $z = 10$ rising to a scatter of ∼0.45 dex at $z = 13$. We adopt the Reed et al. (2007) model specifically because this is lies in the centre of this scatter over the halo mass range of concern. The Reed et al. (2007) model was also specifically determined by simulating haloes at $z = 10-30$ making it ideal for this work.

We model the star-formation efficiency as a function of halo mass, $\epsilon(M_\mathrm{h})$ through the stellar-to-halo mass relation (SHMR). This relates the stellar and halo masses, incorporating the universal baryon fraction, $f_\mathrm{b} = 0.167$, through the relation

$$\frac{M_*}{M_h} = \epsilon(M_\mathrm{h}) f_\mathrm{b}, \tag{1}$$

which assumes that the efficiency, ϵ, is purely dependent on the mass of a galaxy's host dark matter halo. We then adopt a functional form for $\epsilon(M_\mathrm{h})$ using the double power-law relationship from Tacchella et al. (2018):

$$\epsilon(M_\mathrm{h}) = 2\epsilon_0 \left[\left(\frac{M_\mathrm{h}}{M_\mathrm{c}}\right)^{-\beta} + \left(\frac{M_\mathrm{h}}{M_\mathrm{c}}\right)^{\gamma} \right]^{-1}, \tag{2}$$

where ϵ_0 is the peak efficiency, M_c is the characteristic mass (the mass at ϵ_0), β is the low-mass slope, and γ is the high-mass slope. We initially use $(\epsilon_0,\ M_\mathrm{c}/\mathrm{M}_\odot,\ \beta,\ \gamma) = (0.16, 10^{11.7}, 0.9, 0.65)$, as this is the parametrization used in Donnan et al. (2024). This relation is shown by the solid red line in Fig. 1. We also show in Fig. 1 the observational constraints on the $z \simeq 0$ SHMR as compiled by Wechsler & Tinker (2018) with the uncertainty captured by the grey shaded region.

We then also compare our initial adopted relation to the predictions from a number of alternative models. These alternative models cover a large range of efficiencies and include some that are clearly inconsistent with the $z = 0$ relation. It can be seen that Tacchella et al. (2018) assume a significantly greater efficiency (∼1 dex) whereas the model from Mason et al. (2015) is moderately lower and the models from Sun & Furlanetto (2016) and Harikane et al. (2022) are significantly lower. For the semi-analytical model from Yung et al. (2019), we plot their $z = 10$ relation. Another feature of these models is that they assume a rather low efficiency for massive dark matter haloes ($M_h > 10^{11.7}\,\mathrm{M}_\odot$) compared to both our initially adopted model and indeed the relation at $z = 0$. These models had been specifically designed to model the UV LF at $z = 4-10$. However, the UV LF is not a direct tracer of star-formation efficiency as the UV luminosity of a galaxy is dictated by more than simply its stellar mass (e.g. stellar age, star-formation history). Therefore, although these models all assume significantly different star-formation efficiencies, they often still yield similar final UV LFs at $z = 4-10$ due to

Downloaded from https://academic.oup.com/mnras/article/539/3/2409/8116291 by DESY-Zentralbibliothek user on 07 May 2025

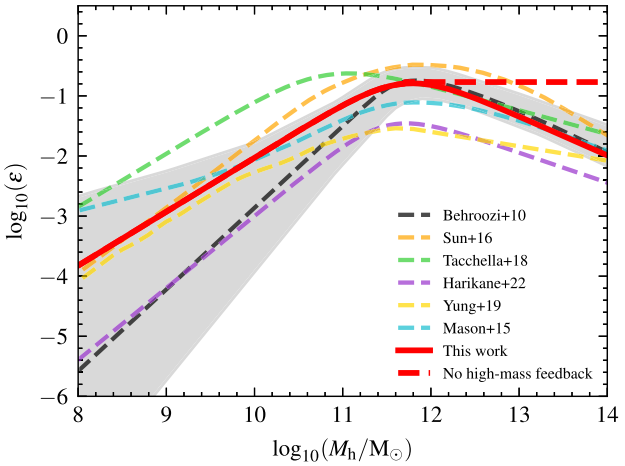


Figure 1. The adopted (redshift independent) star-formation efficiency (ϵ) as a function of halo mass in our model from Donnan et al. (2024) (solid red line) compared to the corresponding relations in the models from Sun & Furlanetto (2016), Tacchella et al. (2018), Harikane et al. (2022), Yung et al. (2019), and Mason et al. (2015). The dashed grey line shows the $z = 0.1$ Behroozi, Conroy & Wechsler (2010) stellar-to-halo mass relation (SHMR) which is identical to the relation adopted here at high masses. The low-mass form of our adopted relation is chosen to better track the observational constraints on the SHMR at $z = 0$ (Wechsler & Tinker 2018), the uncertainty in which is shown here by the grey shaded region. The red dashed line shows our alternative adopted star-formation efficiency (ϵ) model with no high-mass feedback, a model which we explain further in Section 2.3 but ultimately reject in Section 3.

these degeneracies. This is important to note since, as discussed later in Section 6.1, these models have led to claims that a constant star-formation efficiency model fails to reproduce the now well-constrained UV LF at $z > 10$ (e.g. Harikane et al. 2023; Tacchella 2024). However, we re-emphasize here that, as demonstrated in Fig. 1, there are in fact very substantial differences in what form any proposed constant star-formation efficiency is assumed to take.

2.2 Observational constraints on the GSMF

Given that there are such significant differences between the star-formation efficiency relations assumed by different models, breaking the degeneracy between any evolution in the efficiency function and, for example changing mass-to-light ratios in galaxies requires direct tests of the evolving GSMF predicted by the different models. Using the $\epsilon(M_h)$, halo mass can be converted to a stellar mass, M_*, by:

$$M_* = \epsilon(M_h) f_b M_h. \tag{3}$$

The galaxy number density as a function of stellar mass is then given by:

$$\frac{dn}{d\log(M_\star)} = \frac{d\log(M_h)}{d\log(M_\star)} \times \frac{dn}{d\log(M_h)}. \tag{4}$$

Therefore, by assuming a form for the HMF, we can derive a model of the GSMF using a functional form for $\epsilon(M_h)$. This allows measurements of the GSMF to directly establish the star-formation efficiency, hence enabling direct tests of our model as well as those presented in the literature.

With sensitive imaging at $\lambda > 2\,\mu$m, *JWST* now allows robust measurement of the GSMF at $z = 6 - 8$. In Fig. 2, we compare our model prediction for the evolving GSMF at $z = 6 - 8$ to the latest observational measurements from a number of pre-*JWST* (Duncan et al. 2014; Grazian et al. 2015; Stefanon et al. 2021) and now *JWST* measurements (Harvey et al. 2024; Shuntov et al. 2025; Weibel et al. 2024). This demonstrates that our model is able to closely match the observational data points of the GSMF at $z = 6 - 8$. This also confirms that the simple assumption of a star-formation efficiency function unchanged from that observed at $z = 0$ is sufficient to successfully reproduce the GSMF out to the highest redshifts for which robust measurements have so far been achieved. Crucially, however, Fig. 2 also demonstrates that several of the other models in the published literature, while designed to potentially reproduce the $z = 4 - 8$ UV LF, clearly fail this fundamental GSMF test.

2.3 The effect of removing high-mass feedback

Although the star-formation efficiency function used in Donnan et al. (2024) is successfully able to broadly match the observational measurements of the GSMF at $z = 6 - 8$, this $\epsilon(M_h)$ was designed primarily to reproduce the UV LF at $z \geq 9$ where the halo masses of interest lie below the peak of the star-formation efficiency relation (i.e. $\log(M_h/M_\odot) \lesssim 11.7$). Therefore, in that work we simply assumed a high-mass slope equal to that of the $z = 0.1$ SHMR from Behroozi et al. (2010) of $\gamma = 0.65$. However, at $z \geq 7$ there have been suggestions that it may make sense to invoke a lack of high-mass feedback at early times to explain the excess in the bright-end of the UV LF (compared to a Schechter function) through increased star-formation rates at a given halo mass (e.g. Bowler et al. 2017, 2020; Stefanon et al. 2019). Given that the GSMF is a more direct probe of the star-formation efficiency and now that it has been better determined at $z = 6 - 8$, we are able to test if the high-redshift form of the GSMF does indeed require less high-mass feedback than at later times. To explore this we introduce an alternative form of $\epsilon(M_h)$ in which a constant value of $\epsilon(M_h) = 0.17$ is assumed for $\log(M_h/M_\odot) > 11.7$, thus essentially removing all feedback within high-mass haloes. This modification is illustrated in Fig. 1 by the dashed red line which, for simplicity, has the same functional form for $\epsilon(M_h)$ as our original version at lower masses, $\log(M_h/M_\odot) < 11.7$.

From Fig. 2 it can be seen that, for the majority of the stellar mass-range probed by the observational measurements of the GSMF, the removal of high-mass feedback has no effect because these observations probe modest halo masses of $\log(M_h/M_\odot) < 11.7$. However, the highest mass bins at $z = 7$ in particular are more closely matched by our model with high-mass feedback removed. Therefore, one might conclude that there is tentative evidence in favour of the removal of high-mass feedback at $z = 7$.

However, caution is required when comparing to observations of the high-mass end of the GSMF. First, the high-mass end of the GSMF is vulnerable to Eddington bias (Eddington 1913). When measuring the GSMF, each galaxy in the sample has a stellar mass measurement with an associated uncertainty. This means that when measured, galaxies scatter above and below the true stellar mass value. Since there are a lot more low-mass galaxies than high-mass galaxies (as the GSMF declines steeply at high mass), then more of the low-mass galaxies scatter upwards than high-mass galaxies scatter downwards, resulting in an artificial boosting of the number densities of galaxies in the high-mass bins.

Secondly, the galaxy number densities in the highest mass bins are inevitably highly uncertain because they are often based on a very small number of galaxies, or in extreme cases even the proposed presence of a single high-mass source. This is particularly true for the high-mass bins from Shuntov et al. (2025). Therefore, even a small number of contaminants (e.g. due to erroneous photometric

Downloaded from https://academic.oup.com/mnras/article/539/3/2409/8116291 by DESY-Zentralbibliothek user on 07 May 2025

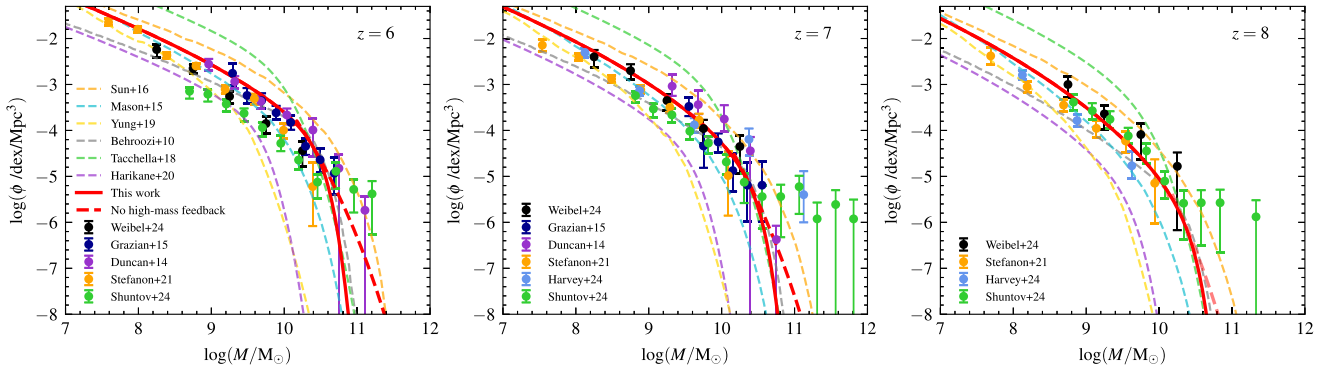


Figure 2. Our model predictions for the evolving galaxy stellar mass function (GSMF) at $z = 6 - 8$ based on the two alternative models of $\epsilon(M_h)$ presented in Fig. 1) are shown in each panel by the red lines (where the dashed version indicates the removal of high-mass feedback). Also shown by data points identified in the legend are the latest observational measurements of the GSMF from Duncan et al. (2014), Grazian et al. (2015), Stefanon et al. (2021), Harvey et al. (2024), Shuntov et al. (2025), and Weibel et al. (2024). The predictions of the GSMF using the alternative $\epsilon(M_h)$ relations shown in Fig. 1 from Tacchella et al. (2018), Harikane et al. (2022), Yung et al. (2019), Sun & Furlanetto (2016), Mason et al. (2015), and Behroozi et al. (2010) are shown by the various fainter coloured dashed lines for comparison. All stellar masses have been adjusted to assume a Chabrier (2003) initial mass function.

redshifts) can drastically change the measured number density at $\log(M_\star/\mathrm{M}_\odot) \gtrsim 10.6$. Ultimately, there are not yet enough confirmed galaxies with $\log(M_\star/\mathrm{M}_\odot) \gtrsim 10.6$ at $z \geq 6$ to place meaningful constraints on the GSMF in this mass range. Increased survey areas with enhanced filter coverage are required to robustly test the need for high-mass feedback through direct comparison with the high-redshift form of the GSMF. In Section 3, we present another test of the need for high-mass feedback using our model of the intrinsic UV LF.

3 THE GALAXY UV LUMINOSITY FUNCTION

3.1 Observational measurements of the UV luminosity function at z = 6 − 13

The next stage of the model is to convert the GSMF into a galaxy UV LF in order to compare our model to observational measurements of the UV LF at $z = 6 - 13$.

The UV LF at $z \geq 6$ has primarily been measured using photometric surveys from space-based telescopes (e.g. *HST*, *JWST*). Prior to the launch of *JWST*, there existed a general consensus over the measured form of the UV LF at $z = 6 - 8$, as described by an evolving Schechter function with a fairly steep faint-end slope of $\alpha \simeq -1.8$ (e.g. Bouwens et al. 2007, 2021; McLure et al. 2009, 2010). However, *HST* data alone were unable to probe the bright-end of the UV LF ($M_{\mathrm{UV}} \lesssim -21.5$) due to the limited area of *HST* surveys. Fortunately, wider-area ground-based surveys were able to probe this luminosity range, hence enabling measurements of the bright-end of the UV LF, at least out to $z \simeq 9$.

Therefore, in this work we include the latest ground-based constraints on the bright-end of the UV LF in combination with a representative fainter data set from space-based surveys at each redshift. This forms the data set that we use to model the UV LF. At $z = 6$ we use the *HST* measurements from Bouwens et al. (2021) with the ground-based data from Bowler et al. (2015). At $z = 7$ we use the data from McLure et al. (2013) in combination with that provided by Bowler et al. (2017) and Varadaraj et al. (2023). At $z = 9$ we use the data from McLure et al. (2013) combined with that from Bowler et al. (2020) and Donnan et al. (2023a). At $z \geq 9$ we use the *JWST* measurements from Donnan et al. (2024) including bright-end constraints at $z = 9$ from Bowler et al. (2020) and Donnan et al. (2023a).

3.2 Modelling the UV luminosity function

To convert our model of the GSMF into a predicted UV LF, we assume a redshift-dependent mass-to-light ratio given by a linear relationship between M_{UV} and $M_\star$:

$$M_{\mathrm{UV}} = M_{\mathrm{UV},*} - 2.5\left[\log_{10}(M_\star/\mathrm{M}_\odot) - 9\right], \quad (5)$$

where $M_{\mathrm{UV},*}$ is the rest-frame UV absolute magnitude corresponding to $\log_{10}(M_\star/\mathrm{M}_\odot) = 9$. This relationship is therefore defined by the UV luminosity which is assumed to be produced by a star-forming galaxy with a stellar mass of $M_\star = 10^9\mathrm{M}_\odot$. To determine this we perform a χ^2 minimization fit to the faint-end of the UV LF data points ($M_{\mathrm{UV}} > -19$) where, at $z = 6 - 13$, the galaxy population can be reasonably expected to be virtually dust-free and therefore the observed UV flux density from these fainter galaxies can be assumed to be unattenuated by dust. The resultant $M_{\mathrm{UV},*}$ required for our model to reproduce the UV LF as a function of redshift is noted in the second column of Table 1. The M_{UV} for a galaxy of a given stellar mass can then be linked to the age of the stellar population within that galaxy, since a younger stellar population at fixed stellar mass has an increased UV luminosity and hence a more negative absolute magnitude.

To determine the stellar age associated with the required M_{UV} for a stellar mass of $\log_{10}(M_\star/\mathrm{M}_\odot) = 9$ at each redshift, we employ stellar population synthesis codes. In this approach, we assume that at a given redshift the average age of a galaxy is independent of it's stellar mass. We use two different codes in this work in order to explore the feasibility of and uncertainty in our approach. First, we use a BC03 stellar population model (Bruzual & Charlot 2003) with a constant star-formation history and a metallicity of $Z = 0.2Z_\odot$. Second, we use THE BINARY POPULATION AND SPECTRAL SYNTHESIS code (BPASS; Eldridge et al. 2017) with a constant star-formation history but with a lower metallicity of $Z = 0.05Z_\odot$. We determine this initially with the stellar continuum only before recalculating the model with an added contribution of the nebular continuum. The relationships between UV magnitude and the stellar mass-weighted age for a galaxy of $\log_{10}(M_\star/\mathrm{M}_\odot) = 9$ for each model

Downloaded from https://academic.oup.com/mnras/article/539/3/2409/8116291 by DESY-Zentralbibliothek user on 07 May 2025

Table 1. The age-dependent UV magnitude mapping to stellar mass as a function of redshift for our model. The first column is the redshift. The second column is the UV absolute magnitude, $M_{\rm UV}$, that corresponds to a stellar mass of $\log(M_*/{\rm M}_\odot) = 9$ determined by the mass-weighted age given in the third column for a BC03 stellar population model (Bruzual & Charlot 2003) with a metallicity of $Z/{\rm Z}_\odot = 0.2$. The fourth column is the inferred mass-weighted age for a BPASS (Eldridge et al. 2017) model with metallicity of $Z/{\rm Z}_\odot = 0.05$ with only a stellar continuum. Finally, the fifth column is the mass-weighted age for a BPASS (Eldridge et al. 2017) model with metallicity of $Z/{\rm Z}_\odot = 0.05$ with both a stellar and nebular contribution to the continuum.

z	$M_{\rm UV}$/AB mag	Age/Myr BC03	Age/Myr BPASS St. only	Age/Myr BPASS St. + Neb.
6	−20.59	140	91	128
7	−20.99	89	58	85
8	−21.03	86	56	82
9	−21.14	75	49	74
10	−21.76	36	24	39
11	−22.74	10	7	14
12.5	−23.27	2.5	3	8

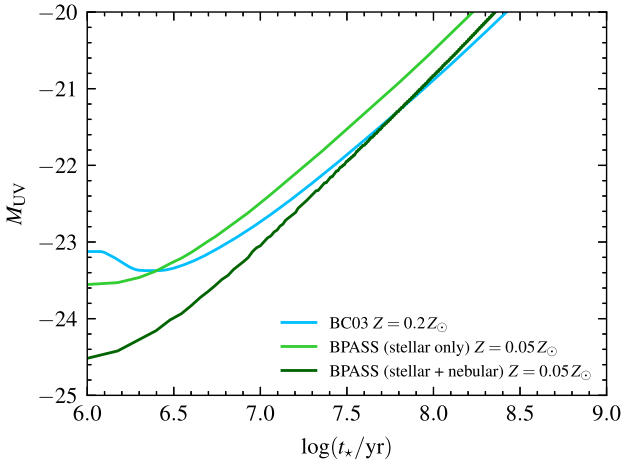


Figure 3. Predicted galaxy UV absolute magnitude as a function of stellar mass-weighted age for a BC03 stellar population model (Bruzual & Charlot 2003) with a constant star-formation history and a metallicity of $Z = 0.2Z_\odot$ (blue), alternatively for a BPASS model (Eldridge et al. 2017) with a constant star-formation history and a metallicity of $Z = 0.05Z_\odot$ with a stellar continuum (light green) and stellar + nebular continuum (dark green).

are shown in Fig. 3. This demonstrates that, for galaxies with ages $\gtrsim 3$ Myr, the stellar only BPASS model consistently produces fainter UV magnitudes whereas this comparison reverses for ages $\lesssim 5$ Myr for the stellar only model. Alternatively, for a given UV magnitude, the BPASS model produces younger stellar ages for $M_{\rm UV} \gtrsim -23$. For the BPASS model with the addition of nebular continuum, the ages are similar to the BC03 model at $M_{\rm UV} \gtrsim -23$ but allow moderately older ages for $M_{\rm UV} \lesssim -23$. For the $M_{\rm UV,*}$ at each redshift, the BC03 and BPASS ages are noted in the latter two columns in Table 1.

3.3 Predictions for high-redshift sub-millimeter galaxies

Using our model of the intrinsic UV LF (i.e. without any dust attenuation, as shown in Fig. 4 at $z = 6, 7, 8, 9, 10, 11, 12.5$) we perform another test of the evidence for and against high-mass feedback in high-redshift galaxies. In this case, we estimate the number of heavily dust-obscured galaxies that would be detectable by sub-mm surveys under either scenario. These are galaxies that contain significant levels of dust attenuation making them extremely faint in the UV and therefore potentially absent from observations of the bright end of the UV LF. However, any such highly star-forming galaxies which are largely attenuated in the rest-frame UV should be revealed at sub-mm wavelengths due to the re-emission of the absorbed UV light by warmed dust grains in the rest-frame far-infrared.

To estimate the prevalence of bright sub-mm sources at high redshifts, inferred from the need to effectively remove them from the bright end of the UV LF through dust obscuration, we proceed as follows.

For simplicity, we consider only galaxies at $z = 6 - 8$ which our model predicts to have an intrinsic unobscured UV absolute magnitude brighter than $M_{\rm UV} = -24.98$. This choice was made in order to capture the number density of galaxies which have an SFR $\geq 300\,{\rm M}_\odot{\rm yr}^{-1}$ according to the conversion factor given by Madau & Dickinson (2014). Specifically, we use the relation:

$$\mathrm{SFR} = \mathcal{K}_{\rm UV}\mathcal{L}_{\rm UV}, \tag{6}$$

where $\mathcal{K}_{\rm UV} = 0.70 \times 10^{-28}$ ${\rm M}_\odot$ ${\rm yr}^{-1}$/erg ${\rm s}^{-1}$ ${\rm Hz}^{-1}$ [adjusted to a Chabrier (2003) initial mass function] and $L_{\rm UV}$ is the UV luminosity.

Next, we exploit the work of Dunlop et al. (2017) who derived a relationship between the infrared-visible SFR and observed flux density at $\lambda = 1.3$ mm ($S_{1.3}$) by fitting the characteristic spectral energy distribution (SED) of the ALMA-detected sources in the Hubble Ultra Deep Field (HUDF) across the wavelength range 24 μm − 1.3 mm giving:

$$\mathrm{SFR}/{\rm M}_\odot{\rm yr}^{-1} \simeq 0.3 S_{1.3}/\mu{\rm Jy}, \tag{7}$$

We then simply assume that the intrinsic UV-derived SFR is equal to the actual infrared-inferred SFR to determine the flux density at 1.3 mm (a very reasonable assumption for highly obscured star-forming galaxies). For SFR $\simeq 300\,{\rm M}_\odot{\rm yr}^{-1}$ we derive a 1.3 mm flux-density estimate of $S_{1.3} \simeq 1.0$ mJy. We then assume a functional form for the shape of the far-infrared SED such that $f_\nu \propto \nu^3$ to determine the equivalent flux density at $\lambda_{\rm obs} = 850$ μm. This results in a value of $S_{850} \simeq 3.6$ mJy which enables comparison to SCUBA-2 surveys which have typically achieved 4σ detections and hence published source catalogues down to this 850 μm flux density (e.g. S2COSMOS, AS2UDS; Simpson et al. 2019; Dudzevičiūtė et al. 2020).

Finally, we then integrate our model of the intrinsic UV LF at $z = 6 - 8$ to a limit of $M_{\rm UV} = -24.98$ to determine the number of galaxies that would be detectable in a 850 μm survey down to a flux density of $S_{850} = 3.6$ mJy.

Downloaded from https://academic.oup.com/mnras/article/539/3/2409/8116291 by DESY-Zentralbibliothek user on 07 May 2025

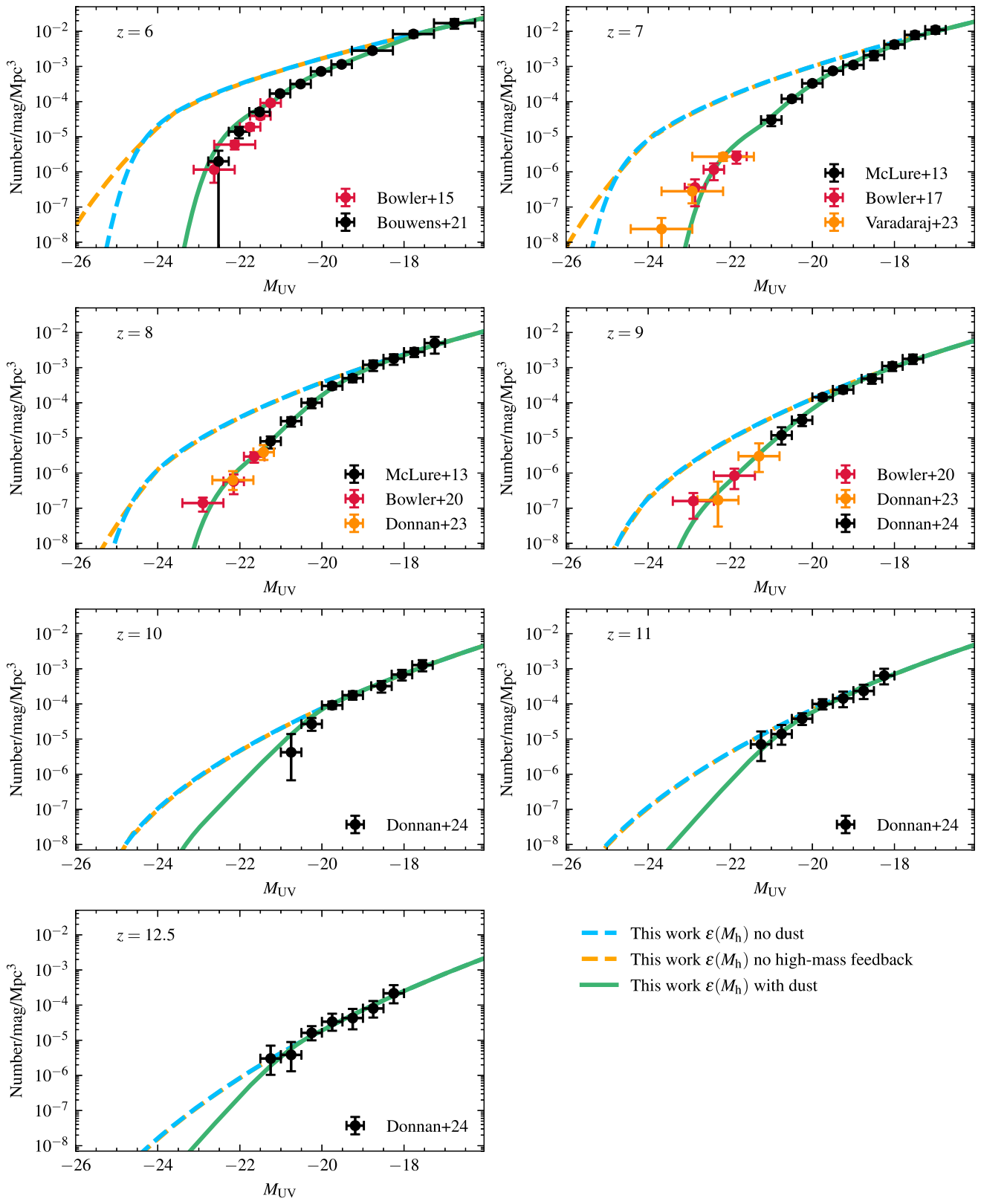


Figure 4. A comparison of our models of the UV luminosity function (UV LF) to observational measurements from McLure et al. (2013), Bowler et al. (2015), Bouwens et al. (2021), Varadaraj et al. (2023), and Donnan et al. (2023a, 2024). The dashed blue line shows our intrinsic dust free model assuming the form of star-forming efficiency $\epsilon(M_h)$ established by Donnan et al. (2024). The dashed orange line shows the dust-free model assuming the Donnan et al. (2024) $\epsilon(M_h)$ model is altered to contain no high-mass feedback. The solid green line shows the final model with dust attenuation.

Downloaded from https://academic.oup.com/mnras/article/539/3/2409/8116291 by DESY-Zentralbibliothek user on 07 May 2025

We compare our model predictions to the AS2UDS survey which detected 364 SMGs across ∼1 deg^2 in the UDS field with $S_{850\mu m} \geq 3.6$mJy based on ALMA follow-up of the original Submillimetre Common-User Bolometer Array 2 (SCUBA-2) Cosmology Legacy Survey of the UDS field (Dudzevičiūtė et al. 2020). They report that two of these sources at $z > 5.5$ indicating a number density of ∼2 galaxies deg^{-2} with $S_{850\mu m} = 3.6$mJy at $z > 5.5$. This is consistent with the more recent *JWST* analysis of the S2COSMOS sample in COSMOS-Web (Casey et al. 2023) which revealed two sources (at $z = 5.5 - 8.5$) across 0.54 deg^2 with a flux density $S_{850} > 2\,mJy$ (McKinney et al. 2025). In this case these two sources have been specifically noted in the literature with AzTECC71 at $z_{phot} = 5.7 \pm 0.6$ (McKinney et al. 2023) and MAMBO-9 at $z_{spec} = 5.850$ (Casey et al. 2019).Their measurements therefore suggest ∼3–4 sources with $S_{850} > 2$ mJy deg^{-2}. Given the somewhat increased depth used in this study compared to our calculation and the presence of an overdensity at $z = 6$ in which one of these sources apparently resides (Brinch et al. 2024), it is consistent with the number density from the AS2UDS survey. We note however, that both the proposed $z > 5.5$ sources in the A2UDS survey only have photometric redshifts, and that our own photometric redshift analysis of this same sample in fact yields no sources with $z > 5.5$. Meanwhile, of the two claimed $z > 5.5$ sources in S2COSMOS sample, only the redshift of AzTECC71 can be considered secure. It is thus reasonable to adopt an estimate of 1 source deg^{-2} with $z > 5.5$ at the $S_{850\mu m} = 3.6$mJy level.

Our model, including continued high-mass feedback (as seen at low redshift) at high redshift yields a prediction of $\simeq 0.3$ galaxies with $S_{850} > 3.6$ mJy deg^{-2}, completely consistent with the available sub-mm survey results. However, with high-mass feedback removed, we predict $\simeq 4$ galaxies with $S_{850} > 3.6$ mJy deg^{-2}, less consistent with the data. Accepting the unavoidable crudeness of this comparison, this demonstrates that the number density of bright sub-mm galaxies can be used to place constraints on the star-formation efficiency in high-mass haloes ($M_h \gtrsim 10^{11.7}$) at early times. In this case the available evidence continues to support the necessity of high-mass feedback, at least out to $z \simeq 6$, or at the very least provides no motivation for increasing efficiency at high masses.

4 DUST ATTENUATION

Given that the intrinsic, dust-free, model is able to successfully reproduce submillimeter number counts, we now consider whether the introduction of a physically plausible relationship between stellar mass and dust attenuation can accurately reproduce the observed UV LF. In Donnan et al. (2024), we accounted for the impact of dust by assuming the $A_{1500} - M_\star$ relation derived for star-forming galaxies at $2 < z < 3$ by McLure et al. (2018). In this study, we attempt to directly measure the $A_{1500} - M_\star$ relation as a function of redshift by forcing agreement between the intrinsic, dust-free, UV LF model and the observed data (as shown in Fig. 4).

To determine the level of UV attenuation as a function of stellar mass, we calculate the difference between the intrinsic model of the UV LF and the observational data at the corresponding number density. The resulting predictions for the $A_{1500} - M_\star$ relation as a function of redshift are shown in Fig. 5, along with the $z \simeq 2.5$ relation from McLure et al. (2018).

Due to the double power law (DPL) functional form used to fit the observed UV LF, our adopted method produces a physically unrealistic turn-over in the derived $A_{1500} - M_\star$ relation at stellar masses of $\log(M_\star/M_\odot) \simeq 10$, corresponding to absolute UV magnitudes well beyond the bright end of the observed UV LF data. Consequently, at each redshift, we implement a horizontal extrapolation at stellar masses greater than the peak of the derived $A_{1500} - M_\star$ curve. This extrapolation, shown as the dashed lines in Fig. 5, begins at $\log(M_\star/M_\odot) \simeq 10$ for redshifts $z = 6 - 9$ and at $\log(M_\star/M_\odot) \simeq 9.9, 9.8, 9.6$ for $z = 10$, 11 and 12.5, respectively. The final UV LF models, incorporating the derived dust attenuation at each redshift, are plotted as the solid green lines in Fig. 4. By design, there is good agreement between the models and the observational data points across the range of UV magnitudes constrained by the available data.

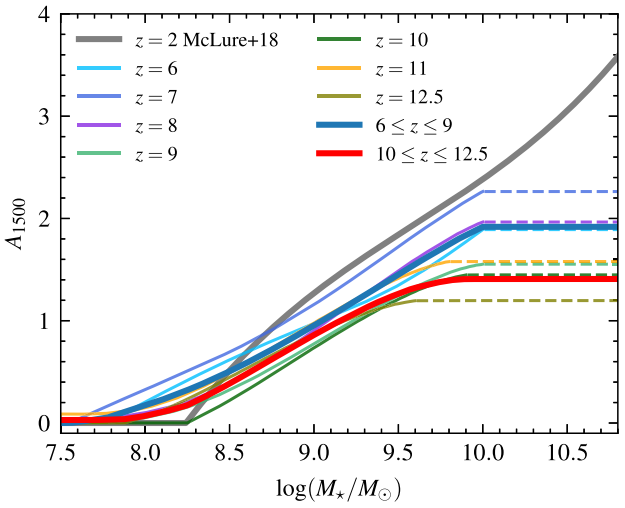


Figure 5. The UV dust attenuation at $\lambda_{rest} = 1500$ Å as a function of stellar mass derived in our model at each redshift. The $z = 2$ relation from McLure et al. (2018) is shown by the solid grey line. The dashed lines show the horizontal extrapolation at high stellar masses. The thick solid blue line shows the mean $A_{1500} - M_\star$ relation at $6 \leq z \leq 9$ whereas the thick solid red line shows the mean $A_{1500} - M_\star$ relation at $10 \leq z \leq 12.5$.

The individual redshift relations for $A_{1500} - M_\star$ shown in Fig. 5 do not display a clear monotonic evolution with redshift although, at fixed stellar mass, there is a tentative trend towards lower dust attenuation at earlier times. This trend is made clearer when considering the mean $A_{1500} - M_\star$ relations in the range $6 \leq z \leq 9$ and $10 \leq z \leq 12.5$, shown as the solid blue and red curves, respectively. Given the uncertainties involved, it is difficult to draw any firm conclusions on the functional form of the derived $A_{1500} - M_\star$ relations. However, they appear physically plausible and, at least within the stellar-mass range that is best constrained by the available data (i.e. $8.5 \leq \log(M_\star/M_\odot) \leq 9.5$), have a similar gradient to the $z \simeq 2.5$ relation from McLure et al. (2018) which was derived using a completely different method.

5 COSMIC HYDROGEN REIONIZATION

Constraining the timeline of reionization continues to be a key goal of extragalactic astronomy. Although there is general consensus that reionization was completed by $z \simeq 5.5 - 6$ (Robertson et al. 2015; Bosman et al. 2021), the evolution of the neutral hydrogen fraction ($X_{H\,I}$) at higher redshifts is still open to question. Fundamentally, the timeline of reionization is governed by the balance between the rate at which ionizing photons are produced and escape into the intergalactic medium (IGM) and the hydrogen recombination rate. The rate at which ionizing photons escape into the IGM is given by:

$$\dot{n}_{ion} = f_{esc}\xi_{ion}\rho_{UV}, \quad (8)$$

Downloaded from https://academic.oup.com/mnras/article/539/3/2409/8116291 by DESY-Zentralbibliothek user on 07 May 2025

where $f_{\rm esc}$ is the escape fraction of Lyman continuum radiation, $\xi_{\rm ion}$ is the ionizing photon production efficiency, and $\rho_{\rm UV}$ is the UV luminosity density. Consequently, by performing a luminosity–weighted integral of our UV LF models to measure $\rho_{\rm UV}$, it is possible to estimate $\dot{n}_{\rm ion}$ as a function of redshift, based on assumed values of $f_{\rm esc}$ and $\xi_{\rm ion}$. When calculating $\rho_{\rm UV}$, we integrate our UV LF models to a common limit of $M_{\rm UV} = -13$, as is typically done when estimating the contribution of the growing galaxy population to cosmic hydrogen reionization (e.g. Robertson et al. 2015; Muñoz et al. 2024; Whitler et al. 2025).

Pre-*JWST*, a canonical value of $\xi_{\rm ion} \simeq 10^{25.2}$Hz erg^{-1} was typically assumed for reionization calculations (e.g. Robertson et al. 2015; Bouwens et al. 2016; Matthee et al. 2017). In contrast, initial *JWST* results suggested that high-redshift galaxies displayed higher efficiencies; $\xi_{\rm ion} \simeq 10^{25.8}$Hz erg^{-1} (e.g. Atek et al. 2024; Simmonds et al. 2024b). However, more recent *JWST*-based studies have tended to revise-down estimates of $\xi_{\rm ion}$, closer to typical pre-*JWST* values (Begley et al. 2024; Pahl et al. 2025; Simmonds et al. 2024a). In order to span the range of observational constraints, in our calculations we adopt three different values of $\xi_{\rm ion}$ with $\log(\xi_{\rm ion}/{\rm Hz\,erg^{-1}}) = 25.2, 25.5, 25.8$.

In a similar fashion, we also consider three different values of $f_{\rm esc}$. At the highest redshifts where it is possible to directly measure $f_{\rm esc}$ (i.e. $3 < z < 3.5$), recent studies based on both photometry and spectroscopy have suggested typical values of $f_{\rm esc} \simeq 0.05$ (e.g. Pahl et al. 2021; Begley et al. 2022). At higher redshifts, estimates of $f_{\rm esc}$ are typically based on the relationship between $f_{\rm esc}$ and the UV slope (β) established at low-redshift (Chisholm et al. 2022). Cullen et al. (2024) report an average UV slope of $\beta = -2.22$ at $z \simeq 10$, corresponding to $f_{\rm esc} = 0.07$ using the relationship from Chisholm et al. (2022). They also report an average UV slope of $\beta = -2.6$ at $z \simeq 11.8$, indicating an increase in escape fraction with redshift to $f_{\rm esc} = 0.19$. Given this range of escape fractions, we determine our model of the neutral fraction as a function of redshift for three fixed values of $f_{\rm esc} = 0.05, 0.10, 0.20$. In addition, we also consider an evolving $f_{\rm esc}$ model, based on the UV slope measurements from Cullen et al. (2024).

Armed with our calculated values of $\dot{n}_{\rm ion}$, we determine the neutral fraction of the IGM by solving the Madau, Haardt & Rees (1999) differential equation governing the change in the ionized fraction of the universe with time:

$$\frac{{\rm d}X_{\rm H\,II}}{{\rm d}t} = \frac{\dot{n}_{\rm ion}}{\langle n_{\rm H}\rangle} - \frac{X_{\rm H\,II}}{t_{\rm rec}}, \tag{9}$$

where $X_{\rm H\,I}$ is the fraction of ionized hydrogen (and hence the neutral fraction is given by $X_{\rm H\,I} = 1 - X_{\rm H\,II}$), $\langle n_{\rm H}\rangle$ is the average comoving number density of hydrogen and $t_{\rm rec}$ is the time-scale of recombination. This last parameter is defined by:

$$t_{\rm rec} = [{\rm C_{H\,II}}\alpha_{\rm B}(T) n_{\rm e}(1+z)^3]^{-1}. \tag{10}$$

Here, $\alpha_{\rm B}(T)$ is the case-B recombination coefficient, which we assume is $2.59 \times 10^{-13}\,{\rm cm^3\,s^{-1}}$ given $T = 10^4$ K, and $C_{\rm H\,II}$ is the IGM clumping factor, which we assume follows the redshift-dependent form provided by Shull, Smith & Danforth (2012). The resulting evolution of $X_{\rm H\,I}$ with redshift corresponding to our different parameter choices is shown in Fig. 6, along with the latest observational constraints from the literature.

It can be seen from Fig. 6 that different choices of $f_{\rm esc}$ and $\xi_{\rm ion}$ have a significant impact on the timeline of reionization. For $f_{\rm esc} = 0.2$, we find that reionization completes by $z = 7$, for all but the lowest considered ionizing photon production efficiency ($\log(\xi_{\rm ion}/{\rm Hz\,erg^{-1}}) = 25.2$). In contrast, if we adopt $f_{\rm esc} = 0.1$, reionization is only able to complete by $z \simeq 6$ assuming $\log(\xi_{\rm ion}/{\rm Hz\,erg^{-1}}) = 25.8$. If we further reduce the assumed escape factor to $f_{\rm esc} = 0.05$, then it can be seen that reionization can only be completed by $z \simeq 6$ for an adopted ionizing photon production efficiency of $\log(\xi_{\rm ion}/{\rm Hz\,erg^{-1}}) \geq 25.8$. Finally, using the evolving prescription for $f_{\rm esc}$, reionization also only ends by $z \simeq 6$ for $\log(\xi_{\rm ion}/{\rm Hz\,erg^{-1}}) \geq 25.8$ (due to the relatively low value of $f_{\rm esc}$ across most of the relevant redshift range).

6 DISCUSSION

6.1 A constant star-formation efficiency

We have presented a simple theoretical model which is able to match the observational constraints on both the GSMF at $z = 6 - 8$ and the UV LF at $z = 6 - 13$ (i.e. out to the highest redshifts for which robust measurements of these two key scaling relations currently exist). This was achieved using a redshift-independent form of the SHMR and therefore a redshift-independent form of the star-formation efficiency (as a function of halo mass) that is consistent with that observed at $z = 0$. We first describe this model in the context of the GSMF and then the UV LF.

6.1.1 Modelling the GSMF with constant star-formation efficiency

First, we tested our constant efficiency model against recent measurements of the evolving GSMF, finding good consistency with the observationally derived data points. The viability of a non-evolving star-formation efficiency is also consistent with several pre-*JWST* measurements of the GSMF obtained through abundance matching (Behroozi, Wechsler & Conroy 2013; Stefanon et al. 2021) as well as the predictions of at least some simulations (Feldmann et al. 2025). However, arguments have also been advanced in support of a redshift-dependent star-formation efficiency, based both on new observations (Shuntov et al. 2025) and alternative simulations (Ceverino et al. 2024). None the less, across most of the mass range, the evolution with redshift that has been suggested has been relatively mild, with even the evolving efficiency functions generally lying within the scatter of the $z = 0$ relation.

Recently, however, claims have been advanced that the GSMF requires significantly increased star-formation efficiency at $z > 6$ for the most massive galaxies. In particular, Shuntov et al. (2025) make the dramatic claim that, at the highest redshifts, star-formation efficiency rises to $\epsilon = 0.8 - 1.0$ for $\log(M_\star/{\rm M_\odot}) > 10.8$. However, this conclusion is based on highly uncertain high-mass data points which are particularly vulnerable to contamination and bias, for example due to incorrect photometric redshifts (especially likely in this study due to the currently limited filter set of the COSMOS-Web imaging). In addition to the positive bias at the high-mass end resulting from even a tiny number of incorrect photometric redshifts, and the inevitability of Eddington bias (Eddington 1913), it has also been demonstrated that the use of NIRCam photometry alone can result in the stellar masses of some galaxies being overestimated by up to $\simeq 0.5$ dex (Wang et al. 2024).

Finally, while the robust measurement of the GSMF is currently limited to $z \leq 8$ due to the requirement of sufficiently long wavelength coverage red-ward of the Lyman break, we note that this has not deterred several authors from providing measurements at $z = 9 - 11$, which have again in some cases been used to

Downloaded from https://academic.oup.com/mnras/article/539/3/2409/8116291 by DESY-Zentralbibliothek user on 07 May 2025

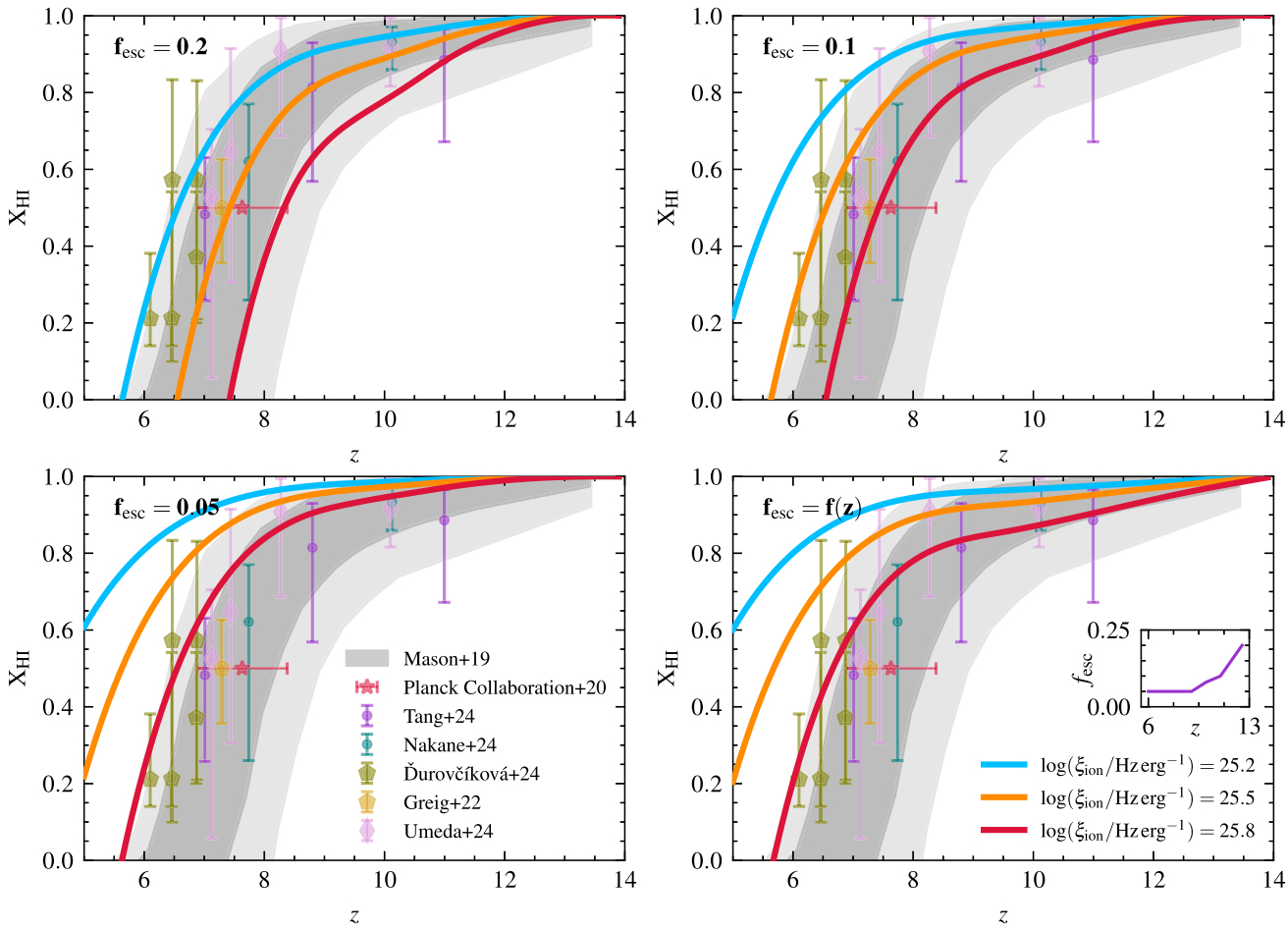


Figure 6. The redshift evolution of the hydrogen neutral fraction of the intergalactic medium with our model predictions given by the solid blue, orange, and red lines for $\log(\xi_{ion}/\mathrm{Hz\,erg^{-1}}) = 25.2, 25.5, 25.8$, respectively where the UV LF is integrated to a limit of $M_{UV} = -13$. In each panel the models are computed using different escape fractions with $f_{esc} = 0.2$ (upper left), $f_{esc} = 0.2$ (upper right), $f_{esc} = 0.05$ (bottom left), and for an evolving f_{esc} as function of redshift (bottom right and inset). Observational measurements of the neutral fraction are shown for the cosmic microwave background (CMB) (Planck Collaboration VI 2020), Lyα equivalent widths (Nakane et al. 2024; Tang et al. 2024), quasar damping wings (Greig et al. 2022; Ďurovčíková et al. 2024), and for Lyman break galaxy (LBG) damping wings (Umeda et al. 2024). The grey shaded region shows the model from Mason et al. (2019) (dark grey: 68th percentile; light grey: 95th percentile).

argue for increased star-formation efficiency (Harvey et al. 2024; Shuntov et al. 2025; Weibel et al. 2024). Although these tentative estimates are not shown in Fig. 2, we have checked that, within the observational uncertainties, our model does in fact successfully reproduce the proposed form of the GSMF at $z = 9$ and $z = 11$.

We therefore conclude that, at present, the available observational constraints on the evolving GSMF provide no clear evidence for a significant increase in star-formation efficiency in massive galaxies at $z \geq 6$.

6.1.2 *The cosmic stellar mass density at $z = 6 - 13$*

A useful global property that can be determined from the GSMF is the evolving cosmic stellar-mass density, $\rho_\star$, which describes the stellar mass per unit comoving volume as a function of redshift. This is determined by the mass-weighted integral of the GSMF given by:

$$\rho_\star = \int_{M_1}^{M_2} M_\star \phi(M_\star, z) d M_\star, \tag{11}$$

where stellar mass is given by $M_\star$, the GSMF is given by $\phi(M_\star, z)$, and M_1, M_2 define the chosen integration limits. Here, we adopt $M_1 = 10^8\,\mathrm{M}_\odot$ and $M_2 = 10^{13}\,\mathrm{M}_\odot$ as typically assumed in observational studies of the GSMF. In Fig. 7, we show the resulting prediction of our model (red line) in comparison to the observational measurements from Duncan et al. (2014), Grazian et al. (2015), Stefanon et al. (2021), Harvey et al. (2024), Shuntov et al. (2025), and Weibel et al. (2024). This demonstrates that our constant star-formation efficiency model is able to successfully reproduce the observed evolution of $\rho_\star$ out to $z \geq 11$ while also highlighting the significant scatter of the current observational determinations. Fig. 7 thus reaffirms that an increase in star-formation efficiency at early times is *not* required to explain the growth of cosmic stellar-mass density at early times.

6.1.3 *Star-formation efficiency and the UV LF at $z = 6 - 13$?*

Using a similar type of model to the one considered here, Harikane et al. (2023) concluded that the assumption of constant star-formation

Downloaded from https://academic.oup.com/mnras/article/539/3/2409/8116291 by DESY-Zentralbibliothek user on 07 May 2025

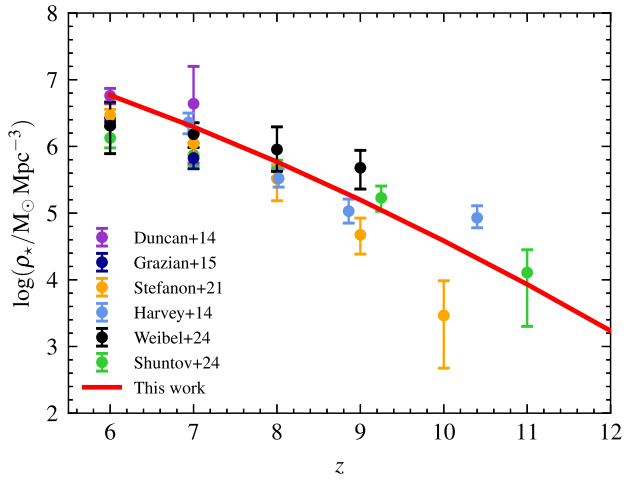


Figure 7. The prediction of our constant star-formation efficiency model for the evolving cosmic stellar-mass density (CSMD), $\rho_\star$, from $z = 6 - 12$ (red). The model prediction is in good agreement with observational constraints from Duncan et al. (2014), Grazian et al. (2015), Stefanon et al. (2021), Harvey et al. (2024), Shuntov et al. (2025), and Weibel et al. (2024). Where necessary, all observational data points have been converted to a Chabrier (2003) initial mass function and are integrated over the mass range $10^8 - 10^{13}$ M$_\odot$.

efficiency was able to reproduce the UV LF out to $z \simeq 10$, but that an increased efficiency was required at still higher redshifts. There have also been a number of other studies suggesting that increased star-formation efficiency is required to explain the form of the UV LF at $z > 10$, especially at the bright end (e.g. Dekel et al. 2023).

Of course, the difficulty in using the UV LF as a measurement of the star-formation efficiency is that the UV luminosity of a galaxy does not simply depend on its stellar mass. Even at early times, a galaxy of a given stellar mass can have a range of UV luminosities dependent on its star-formation history and the age/metallicity of the stellar population that dominates the rest-frame UV. Indeed, in the simple model discussed here we have demonstrated that the assumption of constant star-formation efficiency can be maintained by appealing to ever younger stellar populations to produce an increasing average UV luminosity with increasing redshift beyond $z \simeq 8$. It is only through the flexibility of decreasing typical age at extreme redshifts that our constant-efficiency model is able to explain the UV LF at $z = 10 - 13$.

Somewhat surprisingly, the idea of decreasing characteristic age at extreme redshifts is not regularly cited as an explanation for the observed modest evolution of the UV LF (and hence $\rho_{\rm SFR}$) from $z \simeq 8$ out to $z \simeq 13$. Nevertheless, at some stage young ages become inevitable as we are rapidly running out of time at these redshifts, and indeed our approach is vindicated by the observed consistency of our model (without modification), with measurements of the GSMF (which offers a more direct probe of star-formation efficiency). A key prediction resulting from this trend of younger ages with increasing redshift, is that this trend can continue only for so long as at a certain point, galaxies can no longer be made younger. In fact, the ages at all redshifts in this study are consistent with a formation redshift of $z \simeq 15$, indicating that at $z \gtrsim 15$ there should be a more rapid decline in $\rho_{\rm SFR}$ due to the rapid evolution of the halo mass function.

Finally, we note that while our simple constant-efficiency model can reproduce the UV LF at $z > 10$, more extensive spectroscopy of galaxies at $z > 10$ is required to investigate the physical properties of early galaxies in detail, including the ages of their stellar populations. To date, only a handful of galaxies at such extreme redshifts (extending up to $z = 14.2$) have been observed with NIRSpec (e.g. Arrabal Haro et al. 2023; Bunker et al. 2023; Castellano et al. 2024) and ALMA (Schouws et al. 2024; Zavala et al. 2024), and so it remains unclear how typical their properties are of the wider emerging galaxy population at these early times. Fortunately, in Cycle 3 *JWST* is set to observe an order-of-magnitude more galaxies at $z > 10$ with NIRSpec, through a series of major spectroscopic surveys (e.g. CANDELS-Area Prism Epoch of Reionization Survey (CAPERS) GO 6368).

6.2 No evidence for removing feedback in high-mass haloes

A number of studies have presented evidence for an excess of bright galaxies ($M_{\rm UV} \lesssim -21$) at $z \geq 6$ compared to expectations based on the assumption (well justified at lower redshifts) that the LF follows the exponentially declining form of a Schechter function (e.g. Bowler et al. 2014, 2020; Stefanon et al. 2019).

One possible explanation for this phenomenon is the weakening or removal of high-mass feedback at early times. With feedback reduced or even non-existent at high masses, galaxies can rapidly assemble larger stellar masses and therefore produce greater UV luminosities, thus potentially explaining the observed slow evolution in the bright-end of the UV LF. High-mass feedback is typically explained by the impact of active galactic nuclei (AGNs) in massive galaxies whereby their jets expel gas from the galaxy therefore quenching further star formation, potentially permanently (Hopkins et al. 2006). Alternatively, halo quenching can also act as a feedback mechanism, with the shock-heating of gas in massive haloes effectively removing the reservoir of cold gas required for star formation (Somerville et al. 2008; Gabor & Davé 2015).

It might reasonably be expected that both of these high-mass feedback mechanisms would be less effective at extreme redshifts, with supermassive black holes and high-mass dark matter haloes requiring time to grow. However, as we discussed in Section 3.3 there exists no clear evidence for the removal of high-mass feedback at $z \geq 6$ given the current observational constraints on the evolving GSMF.

This motivated our test of the sub-mm galaxy counts using our model of the intrinsic form of the UV LF. This is a useful test of the high-mass end of star-formation efficiency because it is now well established that the most massive star-forming galaxies are heavily obscured by dust and are thus unlikely to feature even at the bright end of the UV LF (despite obviously still appearing at the high-mass end of the GSMF). We have found that the number of bright high-redshift galaxies observed in current sub-mm surveys (e.g. Simpson et al. 2019; McKinney et al. 2025) also provides little evidence for any decline in high-mass feedback at early times, with the observed prevalence of bright sub-mm galaxies ($\simeq 1$ deg^{-2} at $z > 5.5$ forming stars at a rate $\geq 300\,{\rm M}_\odot{\rm yr}^{-1}$) being completely consistent with the predictions of our fiducial model. Furthermore, in Section 4 we demonstrated that we obtain physically plausible relationships between the UV attenuation and stellar mass for $z \geq 6$ (discussed further in Section 6.3) with an unchanged high-mass star-formation efficiency.

Although in our model the bright end of the UV LF can be fully explained by the level of dust attenuation, and the sub-mm galaxy counts provide some further constraining power, the precise differentiation between weakening star-formation efficiency and increasing dust attenuation will require further observational measurements. Direct measurements of the dust content of galaxies at $z \geq 6$ with ALMA and the Northern Extended Millimeter Array

Downloaded from https://academic.oup.com/mnras/article/539/3/2409/8116291 by DESY-Zentralbibliothek user on 07 May 2025

(NOEMA) will help determine the relationship between stellar mass, UV luminosity, and dust attenuation in these galaxies. This requires both sufficient depth (to be able to detect or robustly constrain the dust continuum) and surveys covering sufficient area in order to detect a statistically significant number of galaxies with stellar masses of $\log(M_\star/\mathrm{M}_\odot) > 10$ at $z \geq 6$.

While our tests of the high-redshift sub-mm galaxy counts do not provide any strong support for the removal of high-mass feedback at early times, currently we cannot precisely determine the normalization and form of the high-mass end of the SHMR at $z \geq 6$. This would require improved measurements of the high-mass end of the GSMF which can only be enabled by yet wider-area NIRCam surveys with *JWST*.

Progress is being made in this direction. To date Harvey et al. (2024) have presented measurements of the GSMF using $\simeq 187$ arcmin^2 of NIRCam imaging, while Weibel et al. (2024) used a larger area of $\simeq 500$ arcmin^2 from the Public Release IMaging for Extragalactic Research (PRIMER; Dunlop et al. 2021), the JWST Advanced Deep Extragalactic Survey (JADES; Eisenstein et al. 2023), and the Cosmic Evolution Early Release Science Survey (CEERS; Bagley et al. 2023).More recently, Shuntov et al. (2025) have presented measurements of the GSMF based on the Cosmos-Web programme (Casey et al. 2023) which significantly expands the available survey area to $\simeq 0.5$ deg^2. However, as discussed above, the COSMOS-Web survey is currently limited to only 4 NIRCam filters (*F*115*W*, *F*150*W*, *F*277*W*, *F*444*W*) which results in significantly less robust photometric redshifts and estimated stellar masses. The upcoming *JWST* Cycle-3 COSMOS-3D programme (PI: Kakiichi) will provide *F*200*W* and *F*356*W* imaging across $\sim$0.33 deg^2 of the COSMOS-Web footprint therefore providing contiguous NIRCam wavelength coverage from 1 to 44 μm which should provide significantly improved stellar mass constraints for the galaxies detected in this field.

Finally, another important consideration is the wavelength coverage of the observations. Interestingly, Wang et al. (2024) used the JWST Mid Infrared Instrument (MIRI) imaging at 7.7 μm to extend the wavelength coverage used to measure galaxy stellar masses beyond that which can be accessed with NIRCam. They concluded that this has an important impact in the sense that the inclusion of the MIRI data results in a significant reduction in the observed number densities of massive galaxies. Therefore, the robust determination of the GSMF at $z > 6$ will require further expansion of the existing *JWST* imaging surveys, ideally with substantial NIRCam and MIRI overlap (as was designed for PRIMER).

6.3 The evolution of the UV attenuation–stellar mass relation

Our model-derived form of the $A_{1500} - M_\star$ relations at $z \geq 6$ as shown in Fig. 5 appear to show some evidence for some modest redshift evolution, with a slightly lower normalization than seen in the $z = 2$ relation derived by McLure et al. (2018). However, the evidence for a change is not compelling, and perhaps more interesting is the extent to which the derived relations still appear to mirror the form of the $z \simeq 2$ relation out to the highest redshifts. This might be regarded as surprising, given that a (relative) lack of dust attenuation in bright ($M_{\mathrm{UV}} \lesssim -21$) galaxies at $z > 10$ has been suggested as an explanation for their observed luminosity (e.g. Ferrara et al. 2023). Moreover, there is also growing evidence from the analysis of the UV continuum slopes exhibited by extreme-redshift galaxies for a transition towards very little or even zero dust attenuation at $z \geq 11$ (e.g. Morales et al. 2023; Topping et al. 2023; Cullen et al. 2024).

However, it transpires that the galaxies uncovered to date at $z \geq 11$ cannot yet settle the issue of whether dust is present or absent at such early times. This is because, as can be seen in Fig. 4, the brightest bin sampled in our analysis of the UV LF at $z \simeq 11$ lies at $M_{\mathrm{UV}} = -21.25$ which, within our model, corresponds to a stellar mass of $10^{8.4}$ M$_\odot$. As can be seen from Fig. 5, at such modest stellar masses (and at all lower stellar masses) negligible dust extinction would be expected even at $z \simeq 2$. As a result, the observed UV LF shown in Fig. 4 is actually consistent with both dusty and dust-free models. In reality, the current observational constraints on dust attenuation in individual galaxies at $z \geq 11$ remain sparse. For example a number of spectroscopically confirmed galaxies at $z \geq 11$ indicate negligible levels of dust attenuation at $M_{\mathrm{UV}} \leq -20$ (e.g. Bunker et al. 2023; Castellano et al. 2024), but spectroscopic observations of a galaxy at $z = 14.3$ hint at some modest (albeit highly uncertain) obscuration ($A_{\mathrm{V}} \simeq 0.3$; Carniani et al. 2024a). Wider area surveys, still deep enough to detect galaxies at $z \simeq 11$, are thus required to properly sample the bright end of the UV LF at these redshifts, uncovering rarer, more massive galaxies. Only then will it be possible to determine whether dust remains prevalent in higher mass galaxies at $z \simeq 11$ and indeed whether the $A_{1500} - M_\star$ relation at these early times is significantly different from that seen at cosmic noon.

A number of other theoretical models have been developed which attempt to predict the dust properties of galaxies at $z > 10$. For example Ferrara et al. (2023) and Ferrara, Pallottini & Sommovigo (2025) suggest that although moderate levels of dust are produced, this dust is removed by radiation-driven outflows. They suggest that such dust removal is required to match the blue colours of early galaxies due to the compact nature of galaxies at $z \geq 11$, as a result of which even a relatively small mass of dust might be expected to produce significant attenuation. Recent ALMA and NOEMA observations of GS-z14 and GN-z11, respectively have attempted to directly determine the dust mass through measurement of the dust continuum in the sub-mm (Fudamoto et al. 2024; Schouws et al. 2024; Carniani et al. 2025). However, these measurements lacked sufficient depth to exclude dust at the level implied by the current models. Significantly deeper ALMA observations are therefore required to directly constrain the levels of dust in galaxies at $z \geq 11$.

6.4 Is there an ionizing photon budget crisis?

Recent *JWST* results have been interpreted by some as suggesting that there may be an ionizing photon budget 'crisis' (Muñoz et al. 2024), in the sense that too many ionizing photons are emitted from the galaxy population at $z > 6$ to be consistent with other constraints on the progress of cosmic hydrogen reionization. This suggestion has arisen in part due to assumptions made regarding the values of the three parameters contained in equation (8), to which the inferred reionization history is sensitive.

JWST has unlocked the ability to measure ξ_{ion} at $z > 6$ for the first time. Early *JWST* results indicated that ξ_{ion} increased as a function of redshift, perhaps reaching significantly higher values of $\log(\xi_{\mathrm{ion}}/\mathrm{Hz\,erg^{-1}}) \simeq 26$ at $z > 6$ (Atek et al. 2024; Simmonds et al. 2024b). This was in part justified by an expectation that the increased burstiness of star formation at early times would result in an increase in the production of ionizing photons. However, recent deeper surveys have led to lower inferred values more typical of what had been established at lower redshifts pre-*JWST*, with various studies now concluding in favour of a more mild evolution with redshift and an average efficiency of $\log(\xi_{\mathrm{ion}}/\mathrm{Hz\,erg^{-1}}) \simeq 25.3$

Downloaded from https://academic.oup.com/mnras/article/539/3/2409/8116291 by DESY-Zentralbibliothek user on 07 May 2025

(Begley et al. 2024; Pahl et al. 2025; Simmonds et al. 2024a). This change in stance may be explained by the fact that the galaxies in earlier studies were selected due to the strengths of key emission lines (e.g. Hα, [O III]) and therefore only provided measurements of $\xi_{\rm ion}$ for the sub-set of galaxies experiencing the strongest bursts of star formation.

The second factor that led to the suggestion of an ionizing photon budget crisis is the assumed value of the typical escape fraction for ionizing photons, $f_{\rm esc}$. For example Muñoz et al. (2024) assume an initial value of $f_{\rm esc} = 0.2$ simply because this was the value adopted in Robertson et al. (2015) as that which was required to complete reionization by $z \simeq 5.5$ (given the other constraints available at that time). Using $f_{\rm esc} = 0.2$, as shown in the upper left panel of Fig. 6, we find consistency with the suggestion from Muñoz et al. (2024) that this *can* result in an excess of ionizing photons leading to premature reionization, with the highest $\xi_{\rm ion}$ model completely reionizing the hydrogen in the IGM by $z \simeq 7.5$. However, pre-*JWST* observational measurements of $f_{\rm esc}$ indicated a significantly lower typical value of $f_{\rm esc} \simeq 0.05$, based on attempted measurements at lower redshifts (Pahl et al. 2021; Begley et al. 2022; Saldana-Lopez et al. 2022). Using the $\beta - f_{\rm esc}$ relation from Chisholm et al. (2022) in combination with recent measurements of β up to $z \simeq 13$ from Cullen et al. (2024), we therefore also calculate the predictions of the model assuming an evolving $f_{\rm esc}$ in which (as implied by the new UV slope measurements) $f_{\rm esc} \simeq 0.2$ at $z = 12$, but then rapidly decreases to $f_{\rm esc} \simeq 0.07$ by $z = 10$ (shown in the inset panel in the bottom right of Fig. 6). However, this change in fact results in a tension with observational constraints on the neutral fraction for even modestly large values of the ionizing production efficiency ($\log(\xi_{\rm ion}/{\rm Hz\,erg^{-1}}) = 25.5$). This is because, based on the values inferred from the evolution of UV continuum slopes, the escape fraction only rises to $f_{\rm esc} = 0.2$ at $z > 10$ and therefore the majority of the reionization history occurs while galaxies have significantly lower escape fractions ($f_{\rm esc} \simeq 0.05$). However, we stress that this tension is in the opposite direction to that proposed by Muñoz et al. (2024), as this model actually lacks the number density of ionizing photons required to complete reionization by $z \sim 6$.

The final parameter that can lead to a predicted excess in the number of ionizing photons is the UV luminosity density, $\rho_{\rm UV}$, produced by the emerging population of young galaxies. This concern was raised in part due to the excess in the observed UV LF compared to some pre-*JWST* models at $z > 10$ (e.g. Mason et al. 2015; Yung et al. 2019). However, our model, which closely reproduces the observed UV LF and $\rho_{\rm UV}$ at $z = 6 - 13$ shows that, in fact, this is not in tension with observational measurements of the neutral fraction including the (now well constrained) end-point of reionization (at $z \simeq 5.5$; Bosman et al. 2021). The calculation of $\rho_{\rm UV}$ is highly sensitive to the limit of the luminosity weighted integral and hence also to the steepness of the faint-end slope of the UV LF, α. Prior to the launch of *JWST*, a range of data provided evidence for a monotonic steepening in α with increasing redshift. In Bouwens et al. (2021), this evolution was described by a linear relationship with redshift, specifically $\alpha = -1.94 - 0.11(z - 6)$ (see Fig. 8). Extrapolation of this linear relationship then provided a prediction of very steep faint-end slopes at $z > 10$. Indeed, assuming this linear extrapolation means that by $z = 11$ one would anticipate a faint-end slope of $\alpha \simeq -2.5$ (Bouwens et al. 2023), significantly steeper than is observed at $z \simeq 8$ ($\alpha \simeq -2.1$).

Early *JWST* measurements of the UV LF were unable to constrain α given the initial lack of ultradeep NIRCam imaging. However, more recent measurements using the JADES (Eisenstein et al. 2023) and the Next Generation Deep Extragalactic Exploratory Public (NGDEEP; Bagley et al. 2024) surveys have enabled a first meaningful attempt at this measurement, yielding $\alpha \simeq -2.2$ to $\alpha \simeq -2.4$ at $z = 11$, albeit still with significant uncertainties (Leung et al. 2023; Pérez-González et al. 2023; Donnan et al. 2024; Whitler et al. 2025). This suggests a significant softening in the evolution in α with increasing redshift compared to some of the aforementioned pre-*JWST* predictions and indeed a plateauing of the faint-end slope around a value of $\alpha \simeq -2.1$ is a clear prediction of our model. This is demonstrated in Fig. 8, where we compare the results of simple power-law fits to the faint end of our evolving model UV LF with existing observational constraints on α at extreme redshifts.

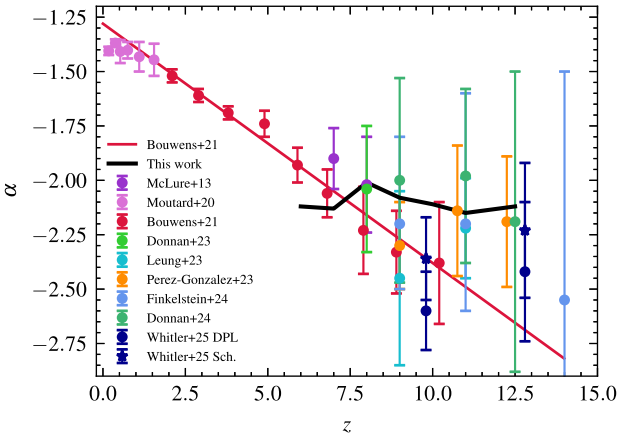


Figure 8. The redshift evolution of the faint-end slope, α, of the galaxy UV LF. The solid red line shows the model from Bouwens et al. (2021) whereas the solid black line shows the faint-end slope predicted by our model as measured over the luminosity range corresponding to $-18.5 < M_{\rm UV} < -17.5$. We also plot a range of observational measurements from McLure et al. (2013), Moutard et al. (2020), Bouwens et al. (2021), Leung et al. (2023), Pérez-González et al. (2023), Donnan et al. (2023a, 2024), Finkelstein et al. (2024), and Whitler et al. (2025). Clearly direct observational constraints on α currently remain very weak, but our model predicts that α is expected to plateau around a value of $\alpha \simeq 2$ at extreme redshifts, and should never approach the extremely steep values inferred from extrapolation of pre-*JWST* data (as indicated by the red line).

Our model also predicts that the faint-end slope should actually reduce in steepness as we move to very faint magnitudes as a result of the non-linear faint-end form of the UV LF (resulting from the underlying form of the halo mass function and the assumed ever decreasing star-formation efficiency at lower masses). This is quantified in Table 2, where we tabulate the faint-end slope resulting from simple power-law fits to our evolving model UV LF over the luminosity ranges corresponding to $-18 < M_{\rm UV} < -16$ and $-17 < M_{\rm UV} < -15$. There is some observational evidence for this shape at $z \simeq 2 - 4$ (Parsa et al. 2016) but deeper *JWST* imaging is required to measure this at the highest redshifts.

Our predicted milder evolution in α with increasing redshift *and* the implied decreasing steepness (*i.e.* curvature) of the UV LF as one moves to fainter UV magnitudes both limit the number density of faint galaxies able to contribute to reionization. This, coupled with the latest *JWST* constraints on the escape fraction and ionizing photon production means that, in this study, we find no evidence for an excess of ionizing photons. Rather, as discussed above, we find that many of our models lack the number density of ionizing photons needed to reproduce current observational constraints on the progress

Downloaded from https://academic.oup.com/mnras/article/539/3/2409/8116291 by DESY-Zentralbibliothek user on 07 May 2025

Table 2. The faint-end slope, α, of our UV LF model at $z = 6 - 12.5$, derived by fitting a power-law functional form over a chosen luminosity range. The first column states the redshift of the UV LF. The second column gives the best-fitting faint-end slope to the model obtained by fitting a power law over the UV magnitude range $-18 < M_{\rm UV} < -16$. The final column then gives the best-fitting faint-end slope derived by fitting to the slightly fainter luminosity range corresponding to $-17 < M_{\rm UV} < -15$. It is notable that, in our model, the faint-end slope plateaus around $\alpha \simeq -2$ at the highest redshifts, and actually flattens slightly as one moves towards very faint luminosities.

z	α $-18 < M_{\rm UV} < -16$	α $-17 < M_{\rm UV} < -15$
6	−1.72	−1.66
7	−1.78	−1.71
8	−1.84	−1.78
9	−1.93	−1.87
10	−2.00	−1.93
11	−2.04	−1.97
12.5	−2.16	−2.08

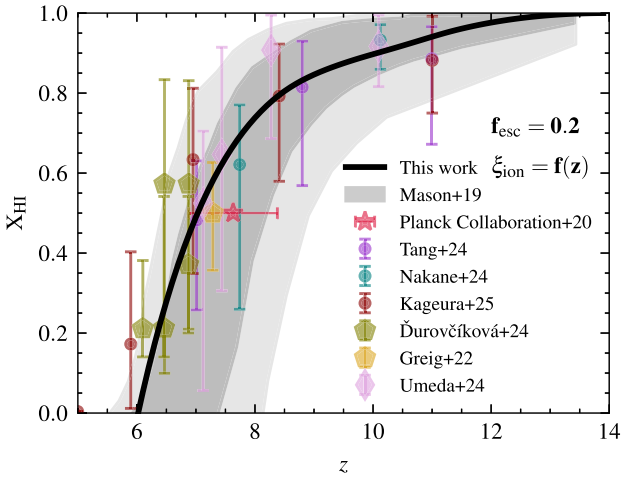


Figure 9. The redshift evolution of the neutral fraction of the intergalactic medium with our final model prediction given by the solid black line where $\log(\xi_{\rm ion}/{\rm Hz\,erg^{-1}}) = 0.035z + 25.08$ (Begley et al. 2024) and the UV LF is integrated to a limit of $M_{\rm UV} = -13$. We assume a fixed $f_{\rm esc} = 0.2$. Observational measurements of the neutral fraction are shown for the CMB (Planck Collaboration VI2020), Lyα equivalent widths (Nakane et al. 2024; Tang et al. 2024; Kageura et al. 2025), QSO damping wings (Greig et al. 2022; Ďurovčíková et al. 2024), and for LBG damping wings (Umeda et al. 2024). The grey shaded region shows the model from Mason et al. (2019) (dark grey: 68th percentile; light grey: 95th percentile).

of cosmic hydrogen reionization unless we adopt a higher escape fraction ($f_{\rm esc} = 0.2$) than required in other studies which assumed steeper faint-end slopes for the LF (e.g. Whitler et al. 2025).

In Fig. 9, we show the final prediction of our model for the redshift evolution of the neutral hydrogen fraction. Here, we use the evolving value of $\rho_{\rm UV}$ calculated from the luminosity weighted integration of our new model UV LF down to $M_{\rm UV} = -13$, assume an escape fraction of $f_{\rm esc} = 0.2$ across the full relevant redshift range, and adopt the redshift-dependent form for $\xi_{\rm ion}$ deduced by Begley et al. (2024). The resulting predicted progress of reionization is clearly consistent with the other available observational constraints plotted in Fig. 9. Crucially, while reionization is predicted to start at quite early times, the model delivers on the now well-established requirement that hydrogen reionization should terminate at $z \simeq 5.5$.

7 CONCLUSIONS

We have developed and tested a simple theoretical model of galaxy evolution with a constant star-formation efficiency, designed in part to check the veracity of recent claims that enhanced star-formation efficiency is required at early cosmological times in order to explain the prevalence of UV luminous galaxies at extreme redshifts, as revealed by *JWST*.

We show that this model, with no free parameters other than mass—light ratio, can indeed perfectly reproduce both the shape and normalization of the galaxy UV LF at $z \simeq 11$, and indeed can match the evolving UV LF over the entire redshift range $z \simeq 6 - 13$, provided we: (i) allow the typical age of the galaxy stellar populations to decrease monotonically from $\simeq 130$ Myr at $z = 6$ to $\simeq 10$ Myr at $z \simeq 13$, and (ii) invoke dust obscuration to explain the form of the UV LF at luminosities brighter than $M_{UV} \simeq -20$ for redshifts $z \leq 10$.

We have also compared the predictions of our model against the latest observations of the evolving GSMF over the redshift range $z \simeq 6 - 8$. The requirement to fit both the UV LF and the GSMF breaks the degeneracy between mass-to-light ratio and star-formation efficiency and we find that our model is consistent with current observational constraints on the GSMF at these epochs, *without alteration or tuning*. This provides reassurance that our assumed non-evolving efficiency is completely consistent with recent *JWST* observations of the young Universe.

We have also explored a modification of our model involving the removal of high-mass feedback at early times which would increase the number of highly star-forming galaxies present in sub-mm surveys. However, the predictions of our *unmodified* model are more consistent with existing constraints from sub-mm surveys, which reveal typically only $\simeq 1$ sub-mm galaxy per square degree with a star-formation rate $\geq 300\,{\rm M_\odot yr^{-1}}$ at $z \geq 6$.

Finally, we have explored the implications of our model for the predicted progress of cosmic hydrogen reionization, in part to test the validity of some recent claims that the latest *JWST* observations suggest early galaxies may emit too many ionizing photons to be consistent with other constraints on reionization. We find that, using the latest measurements of $f_{\rm esc}$ and $\xi_{\rm ion}$ in combination with our model UV LFs, our predictions are not in tension with observational measurements of the timeline of reionization. Our model also predicts that the faint-end slope of the UV LF should plateau at $\alpha \simeq -2.1$ beyond $z \simeq 8$, rather than continuing to steepen at higher redshifts (as often predicted before the advent of *JWST*), a prediction which helps to mitigate any potential ionizing photon crisis.

Because we invoke ever-declining stellar ages (rather than increased star-formation efficiency) to offset the decline in the underlying halo mass function when modelling the extreme-redshift evolution of the UV LF, another clear and *prediction* of our model is that there should be a more rapid drop-off in the galaxy number density galaxies at $z \simeq 15$. It is therefore interesting to note that Donnan et al. (2024) presented tentative evidence for a relatively rapid drop-off in ρ_{UV} at $z \simeq 14.5$ and indeed a compelling galaxy candidate at $z \geq 15$ has yet to be discovered, despite intensive efforts with ever deeper *JWST* data. Time will tell whether $z \simeq 15$ really is the long-sought epoch of galaxy formation, as predicted by our model.

ACKNOWLEDGEMENTS

We thank the referee for their valuable comments which have improved the quality of the manuscript. CTD, DJM, RJM, and JSD acknowledge the support of the Science and Technology

Downloaded from https://academic.oup.com/mnras/article/539/3/2409/8116291 by DESY-Zentralbibliothek user on 07 May 2025

Facilities Council (STFC). JSD also acknowledges the support of the Royal Society through a Royal Society Research Professorship. FC acknowledges support from a UKRI Frontier Research Guarantee Grant (grant reference EP/X021025/1).

DATA AVAILABILITY

The data are available from the authors upon reasonable request.

REFERENCES

Adams N. J., Bowler R. A. A., Jarvis M. J., Varadaraj R. G., Häußler B., 2022, MNRAS, 523, 327
Adams N. J. et al., 2023, ApJ, 965, 169
Arrabal Haro P. et al., 2023, Nature, 622, 707
Atek H. et al., 2024, Nature, 626, 975
Bagley M. B. et al., 2023, ApJ, 965, L6
Bagley M. B. et al., 2024, ApJ, 965, L6
Begley R. et al., 2022, MNRAS, 513, 3510
Begley R. et al., 2025, MNRAS, 537, 3245
Behroozi P. S., Conroy C., Wechsler R. H., 2010, ApJ, 717, 379
Behroozi P. S., Wechsler R. H., Conroy C., 2013, ApJ, 762, L31
Bosman S. E. I., Ďurovčíková D., Davies F. B., Eilers A.-C., 2021, MNRAS, 503, 2077
Bouwens R. J., Illingworth G. D., Franx M., Ford H., 2007, ApJ, 670, 928
Bouwens R. J., Smit R., Labbé I., Franx M., Caruana J., Oesch P., Stefanon M., Rasappu N., 2016, ApJ, 831, 176
Bouwens R. J. et al., 2021, AJ, 162, 47
Bouwens R. J. et al., 2023, MNRAS, 523, 1036
Bowler R. A. A. et al., 2014, MNRAS, 440, 2810
Bowler R. A. A. et al., 2015, MNRAS, 452, 1817
Bowler R. A. A., Dunlop J. S., McLure R. J., McLeod D. J., 2017, MNRAS, 466, 3612
Bowler R. A. A., Jarvis M. J., Dunlop J. S., McLure R. J., McLeod D. J., Adams N. J., Milvang-Jensen B., McCracken H. J., 2020, MNRAS, 493, 2059
Brinch M. et al., 2024, MNRAS, 527, 6591
Bruzual G., Charlot S., 2003, MNRAS, 344, 1000
Bunker A. J. et al., 2023, A&A, 690, A288
Carniani S. et al., 2024a, Nature, 633, 318
Carniani S. et al., 2025, A&A 696 A87
Casey C. M. et al., 2019, ApJ, 887, 55
Casey C. M. et al., 2023, ApJ, 954, 31
Castellano M. et al., 2022, ApJ, 938, L15
Castellano M. et al., 2024, ApJ, 972, 143
Ceverino D., Nakazato Y., Yoshida N., Klessen R. S., Glover S. C. O., 2024, A&A, 689, A244
Chabrier G., 2003, PASP, 115, 763
Chisholm J. et al., 2022, MNRAS, 517, 5104
Chworowsky K. et al., 2024, AJ, 168, 113
Cullen F. et al., 2024, MNRAS, 531, 997
Curtis-Lake E. et al., 2023, Nat. Astron., 7, 622
Dekel A., Sarkar K. C., Birnboim Y., Mandelker N., Li Z., 2023, MNRAS, 523, 3201
Donnan C. T. et al., 2023a, MNRAS, 518, 6011
Donnan C. T., McLeod D. J., McLure R. J., Dunlop J. S., Carnall A. C., Cullen F., Magee D., 2023b, MNRAS, 520, 4554
Donnan C. T. et al., 2024, MNRAS, 533, 3222
Dudzevičiūtė U. et al., 2020, MNRAS, 494, 3828
Duncan K. et al., 2014, MNRAS, 444, 2960
Dunlop J. S. et al., 2017, MNRAS, 466, 861
Dunlop J. S. et al., 2021, PRIMER: Public Release IMaging for Extragalactic Research, JWST Proposal. Cycle 1, ID. #1837
Ďurovčíková D. et al., 2024, ApJ, 969, 162
Eddington A. S., 1913, MNRAS, 73, 359
Eisenstein D. J. et al., 2023, preprint (arXiv:2306.02465)
Eldridge J. J., Stanway E. R., Xiao L., McClelland L. A. S., Taylor G., Ng M., Greis S. M. L., Bray J. C., 2017, PASA, 34, e058
Feldmann R. et al., 2025, MNRAS, 536, 988
Ferrara A., Pallottini A., Dayal P., 2023, MNRAS, 522, 3986
Ferrara A., Pallottini A., Sommovigo L., 2025, A&A, 694, A286
Finkelstein S. L. et al., 2023, ApJ, 946, L13
Finkelstein S. L. et al., 2024, ApJ, 969, L2
Fudamoto Y. et al., 2024, MNRAS, 530, 340
Gabor J. M., Davé R., 2015, MNRAS, 447, 374
Glazebrook K. et al., 2024, Nature, 628, 277
Grazian A. et al., 2015, A&A, 575, A96
Greig B., Mesinger A., Davies F. B., Wang F., Yang J., Hennawi J. F., 2022, MNRAS, 512, 5390
Harikane Y. et al., 2022, ApJS, 259, 20
Harikane Y. et al., 2023, ApJS, 265, 5
Harvey T. et al., 2024, ApJ, 978, 89
Hopkins P. F., Hernquist L., Cox T. J., Di Matteo T., Robertson B., Springel V., 2006, ApJS, 163, 1
Kageura Y. et al., 2025, preprint (arXiv:2501.05834)
Labbé I. et al., 2023, Nature, 616, 266
Leung G. C. K. et al., 2023, ApJ, 954, L46
Madau P., Dickinson M., 2014, ARA&A, 52, 415
Madau P., Haardt F., Rees M. J., 1999, ApJ, 514, 648
Mason C. A., Trenti M., Treu T., 2015, ApJ, 813, 21
Mason C. A., Naidu R. P., Tacchella S., Leja J., 2019, MNRAS, 489, 2669
Matthee J., Sobral D., Best P., Khostovan A. A., Oteo I., Bouwens R., Röttgering H., 2017, MNRAS, 465, 3637
McKinney J. et al., 2023, ApJ, 956, 72
McKinney J. et al., 2025, ApJ, 979, 229
McLeod D. J., McLure R. J., Dunlop J. S., 2016, MNRAS, 459, 3812
McLeod D. J., McLure R. J., Dunlop J. S., Cullen F., Carnall A. C., Duncan K., 2021, MNRAS, 503, 4413
McLeod D. J. et al., 2024, MNRAS, 527, 5004
McLure R. J., Cirasuolo M., Dunlop J. S., Foucaud S., Almaini O., 2009, MNRAS, 395, 2196
McLure R. J., Dunlop J. S., Cirasuolo M., Koekemoer A. M., Sabbi E., Stark D. P., Targett T. A., Ellis R. S., 2010, MNRAS, 403, 960
McLure R. J. et al., 2013, MNRAS, 432, 2696
McLure R. J. et al., 2018, MNRAS, 476, 3991
Morales A. M. et al., 2023, ApJ, 964, L24
Mortlock A. et al., 2015, MNRAS, 447, 2
Moutard T., Sawicki M., Arnouts S., Golob A., Coupon J., Ilbert O., Yang X., Gwyn S., 2020, MNRAS, 494, 1894
Muñoz J. B., Mirocha J., Chisholm J., Furlanetto S. R., Mason C., 2024, MNRAS 535 L37
Murray S. G., Power C., Robotham A. S. G., 2013, Astron. Comput., 3, 23
Muzzin A. et al., 2013, ApJ, 777, 18
Naidu R. P. et al., 2022, ApJ, 940, L14
Nakane M. et al., 2024, ApJ, 967, 28
Oke J. B., 1974, ApJS, 27, 21
Oke J. B., Gunn J. E., 1983, ApJ, 266, 713
Pahl A. J., Shapley A., Steidel C. C., Chen Y., Reddy N. A., 2021, MNRAS, 505, 2447
Pahl A. J. et al., 2025, ApJ, 981,134
Parsa S., Dunlop J. S., McLure R. J., Mortlock A., 2016, MNRAS, 456, 3194
Pérez-González P. G. et al., 2023, ApJ, 951, L1
Planck Collaboration VI, 2020, A&A, 641, A6
Reed D. S., Bower R., Frenk C. S., Jenkins A., Theuns T., 2007, MNRAS, 374, 2
Robertson B. E., Ellis R. S., Furlanetto S. R., Dunlop J. S., 2015, ApJ, 802, L19
Saldana-Lopez A. et al., 2022, A&A, 663, A59
Schouws S. et al., 2024, preprint (arXiv:2409.20549)
Shull J. M., Smith B. D., Danforth C. W., 2012, ApJ, 759, 23
Shuntov M. et al., 2025, A&A, 695, A20
Simmonds C. et al., 2024a, MNRAS, 535, 2998
Simmonds C. et al., 2024b, MNRAS, 527, 6139
Simpson J. M. et al., 2019, ApJ, 880, 43

Downloaded from https://academic.oup.com/mnras/article/539/3/2409/8116291 by DESY-Zentralbibliothek user on 07 May 2025

Somerville R. S., Hopkins P. F., Cox T. J., Robertson B. E., Hernquist L., 2008, MNRAS, 391, 481
Song M. et al., 2016, ApJ, 825, 5
Stefanon M. et al., 2019, ApJ, 883, 99
Stefanon M., Bouwens R. J., Labbé I., Illingworth G. D., Gonzalez V., Oesch P. A., 2021, ApJ, 922, 29
Sun G., Furlanetto S. R., 2016, MNRAS, 460, 417
Tacchella S., 2024, preprint (arXiv:2410.04227)
Tacchella S., Bose S., Conroy C., Eisenstein D. J., Johnson B. D., 2018, ApJ, 868, 92
Tang M., Stark D. P., Topping M. W., Mason C., Ellis R. S., 2024, ApJ,975,208
Topping M. W. et al., 2023, MNRAS, 529, 4087
Umeda H., Ouchi M., Nakajima K., Harikane Y., Ono Y., Xu Y., Isobe Y., Zhang Y., 2024, ApJ, 971, 124
Varadaraj R. G., Bowler R. A. A., Jarvis M. J., Adams N. J., Häußler B., 2023, MNRAS, 524, 4586
Wang T. et al., 2024, preprint (arXiv:2403.02399)
Weaver J. R. et al., 2023, A&A, 677, A184
Wechsler R. H., Tinker J. L., 2018, ARA&A, 56, 435
Weibel A. et al., 2024, MNRAS, 533, 1808
Whitler L. et al., 2025, preprint (arXiv:2501.00984)
Wilkins S. M. et al., 2023, MNRAS, 519, 3118
Yung L. Y. A., Somerville R. S., Popping G., Finkelstein S. L., Ferguson H. C., Davé R., 2019, MNRAS, 490, 2855
Zavala J. A. et al., 2024, ApJL, 977, L9

This paper has been typeset from a TEX/LATEX file prepared by the author.

Downloaded from https://academic.oup.com/mnras/article/539/3/2409/8116291 by DESY-Zentralbibliothek user on 07 May 2025

© 2025 The Author(s).
Published by Oxford University Press on behalf of Royal Astronomical Society. This is an Open Access article distributed under the terms of the Creative Commons Attribution License (https://creativecommons.org/licenses/by/4.0/), which permits unrestricted reuse, distribution, and reproduction in any medium, provided the original work is properly cited.